Organometallic synthesis of ZnO nanoparticles for gas sensing: Towards selectivity through nanoparticles morphology

A. Ryzhikov, J. Jonca, M. L. Kahn, K. Fajerwerg, B. Chaudret, Audrey Chapelle, Philippe Menini, C. H. Shim, A. Gaudon, P. Fau

Organometallic Synthesis of ZnO Nanoparticles for Gas Sensing: Towards Selectivity Through Nanoparticles Morphology.

Andrey Ryzhikov [1], Justyna Jońca [1], Myrtil Kahn [1], Katia Fajerwerg [1,2], Bruno Chaudret [3], Audrey Chapelle [4], Philippe Ménini [2,4], Chang Hyun Shim [4,5], Alain Gaudon [5], Pierre Fau [1,2] *

[1] Laboratoire de Chimie de Coordination (LCC), CNRS, 205 route de Narbonne, 31077 Toulouse Cedex 4, France
[2] Université Toulouse III, Paul Sabatier, 118 route de Narbonne, 31062 Toulouse Cedex 9, France
[3] Laboratoire de Physique et de Chimie de Nano-objets (LPCNO), INSA, UPS, CNRS, 135 avenue de Rangueil, 31077 Toulouse, Cedex 4, France
[4] Laboratoire d'Analyse et d'Architecture des Systèmes (LAAS), CNRS, 5 avenue du Colonel Roche, 31400 Toulouse, France
[5] Alpha MOS, 20 avenue Didier Daurat, 31400 Toulouse, France

* Author to whom correspondence should be addressed;
E-Mail: pierre.fau@lcc-toulouse.fr; Tel.: +33 0561333181; Fax: +33 0561553003

Abstract: ZnO nanoparticles with different morphology such as nanorods (NR), isotropic nanoparticles (NP) and cloud-like (CL) structures have been synthesized by an organometallic route. The prepared ZnO nanostructures have been deposited on miniaturized silicon gas sensor substrates by an ink-jet method, and their responses to CO, C_3H_8 and NH_3 gases have been studied at different operating temperatures (340-500°C) and relative humidity of 50%. It is noteworthy that the morphology of the nanostructure of the sensitive layer is maintained after thermal treatment. The morphology of ZnO nanoparticles significantly influences the sensors response level and their selectivity properties to reducing gases. Among the three different ZnO types, sensors prepared with NR show the highest response to both CO and C_3H_8. Sensors made of isotropic NP and CL structures show a lower but similar to each other response to CO. From all investigated nanostructures, sensors made of CL structures show the weakest response to C_3H_8. With NH_3 gas, no effect of the morphology of the ZnO sensitive layer has been evidenced. These different responses highlight the important role of the nanostructure of the ZnO sensitive layer and the nature of the target gas on the detection properties of the sensors.

Keywords: gas sensor, zinc oxide, morphology influence, nanoparticles, nanorods, crystalline faces, selectivity.

Introduction

Metal oxide semiconductors (MOS) such as SnO_2, ZnO, WO_3 or In_2O_3 are widely studied as sensing materials for resistive type gas sensors due to their high sensitivity, chemical stability and good flexibility in fabrication processes (Simon et al., 2001). The main disadvantage of such sensors is their lack of selectivity since usually all reducing or oxidizing gases react with the metal oxide surface giving rise to a transduction signal. To overcome this drawback, the selectivity to target molecules can be greatly improved by i) the addition of doping elements (Yamazoe et al., 1983), ii) the use of different

heating temperatures, various operating modes of the sensors (Heilig et al., 1997), or iii) the introduction of catalytic filters (Ryzhikov et al, 2005). An enhancement of the sensor selectivity can be also achieved by the combination of different sensing materials and the fine tuning of the operating parameters (heating conditions, temperature cycling …) in multi-sensor devices (Weimar and Goepel, 1998). The morphology control of nanosized MOS can also be envisaged to improve the selectivity towards various gases (. Indeed, it is well established that the surface reactivity of MOS varies depending on their crystalline faces (Cobden et al., 1999). Many studies report that the catalytic activity of the metal oxide nanoparticles can greatly depend on their morphology and the exposed crystalline faces (Chand Singh et al., 2008; Liao et al., 2011; Liu et al., 2011; Wang et al., 2011; Rai et al., 2013; Zhao at al., 2014).

However, the morphology effect on gas sensing properties of semiconducting metal oxide obtained from the same synthetic procedure is rarely described in the literature. The modification of the exposed crystalline faces of $ZnSnO_3$ polyhedral microcrystals have been reported to considerably modify their response to H_2S, HCHO and C_2H_5OH but without significant change of selectivity (Geng et al., 2008). SnO_2, ZnO and In_2O_3 nanostructures have been reported to present different response level to NH_3 gas depending on their shape (*i.e.* nanorods or nanoparticles) (Rout et al., 2007). Gupta and co-workers have shown that ZnO nanotetrapods and nanowires (grown by high temperature evaporation of Zn) possess higher response to H_2S and NO than polycrystalline ZnO films and that the response is mainly determined by intergrain barriers (Gupta et al., 2010). ZnO nanorods with higher response to NO_2 than ZnO nanosheets have recently been reported (Bai et al., 2011). Tungsten oxide nanoplates with higher sensitivity to acetone than WO_3 isotropic nanoparticles have also been described (Chen et al., 2011). The sensing properties of WO_3 nanowires or thin films towards CH_3OH, CO and NO_2 gases are different enough to allow their use in selective multisensor systems (Benkstein et al., 2009). However, SnO_2 nanoparticles with different morphologies have been reported without significant influence on the sensor selectivity (Le et al., 2010; Shaalan et al., 2011, Yu et al., 2011). Importantly, the changes of the sensor response are, in most of the cases, correlated with the specific surface area rather than with the morphology of the nanostructures (Wu et al., 2006; Xu et al., 2008; Zhang et al., 2009). Moreover, the morphology influence on the resulting sensing properties is discussed for the particles having relatively large size (from several tens to several hundred nm). Therefore, the specific surface area of these materials should be relatively low and the final sensor response is rather determined by intergrain boundaries (Goepel and Schierbaum, 1995).

The organometallic synthesis route developed in our team is a rational way to prepare metal and metal oxide nanoparticles of very low size with a well-controlled monodispersity and morphology (Chaudret, 2005). This method consists in low-temperature decomposition of organometallic precursors in organic solvent in the presence of stabilizing agents such as polymers or various ligands. ZnO nanostructures of controlled morphology can be also synthesized by this method (Kahn et al., 2005). One of its principal advantages relies in the control of nanoparticle shape and size without drastic change of the synthesis conditions, so different ZnO nanostructures can be prepared by the same synthetic procedure. As compared to many other methods (Kolodziejczak-Radzimska and Jesionowski, 2014), where high temperatures and/or pressure are required, the preparation of ZnO nanostructures is performed at room temperature and at atmospheric pressure. Therefore, this unique one-pot reaction does not require any special apparatus, leading to simplest and less energy consuming means for preparation of ZnO nanoparticles. In this paper, the synthesis of ZnO nanostructures with different morphologies, from well-defined isotropic nanoparticles to high aspect-ratio nanorods, and the study of their response to three different reducing gases, *i.e.* CO, C_3H_8 and NH_3, are presented. It is therefore possible to compare the

surface reactivity of preferentially exposed crystalline faces. The role of the nanostructure's morphology on the sensors response and selectivity are discussed.

Experimental Section

Synthesis of ZnO nanoparticles

The ZnO nanostructures of different shapes, *i.e.* isotropic nanoparticles (NP), cloud-like nanostructures (CL) and high aspect-ratio nanorods (NR), have been synthesized according to an adapted method from our previous work (Kahn et al. 2005). All nanoparticles have been obtained by the hydrolysis of the same organometallic precursor, namely the dicyclohexylzinc (II) ([ZnCy$_2$], NanoMePS, France, 99% purity). Octylamine (Sigma Aldrich) is used as stabilizing agent. THF is collected from solvent purification system (Braun MB-SPS-800). Distilled water has been degassed with argon during 30 min prior to use. All reactions have been performed at room temperature and under argon atmosphere. In order to prepare ZnO NP, 0.25 mmol dicyclohexylzinc (II) precursor and 0.25 mmol octylamine (1 molar eq. regarding Zn) have been dissolved in 4 mL of THF. In a second step, 2 mL of humidified THF (1 mmol of H$_2$O, 4 molar eq. regarding Zn) has been added dropwise to [ZnCy$_2$] solution. The addition of humidified THF in a limpid [ZnCy$_2$] solution leads rapidly to a yellowish phase. After a few minutes the yellow solution evolves to give rise to a white precipitate. After 16 h of reaction, the nanoparticles have been separated by centrifugation (1000 rpm, 5 min, 20°C) and washed 3 times with 5 mL of acetone (Sigma Aldrich). ZnO CL structures are obtained by following the same procedure but without addition of any surfactant. In order to prepare ZnO NR, a mixture of 0.25 mmol of dicyclohexylzinc (II) and 0.5 mmol (2 molar eq. regarding Zn) of pure octylamine have been introduced into a 4 mL glass flask. The flask has been placed in a flat-bottomed reactor closed with a septum. In a second step, 18 μL (1 mmol, 4 molar eq. regarding Zn) of H$_2$O has been added to the reactor through the septum with a syringe. After 4 days, the nanorods have been dispersed in THF (6 mL). Finally, the nanorods have been separated by centrifugation (1000 rpm, 5 min, 20°C) and washed 3 times with 5 mL of acetone.

ZnO characterization

Transmission Electron Microscopy (TEM), High Resolution Transmission Microscopy (HRTEM) and Scanning Electron Microscopy Field Effect Gun (SEM-FEG) experiments have been carried out respectively on a JEOL JEM 1011, JEOL JEM 2100F and on a JEOL JSM 6700F, at the "Service Commun de Microscopie de L'Université Toulouse III Paul Sabatier". TEM, HRTEM and SEM-FEG images have been used to determine the morphology, particle size, and size distribution. The latter is determined from more than 200 particles of each sample. The obtained ZnO nanoparticles have been studied by X-ray powder diffraction (XRD) on a SEIFERT XRD 300 TT diffractometer operated under Cu Kα radiation, fitted with a diffracted-beam graphite monochromator. The data have been collected in the 2θ configuration between 10 and 70°. Average crystallite size values (FWHM) were calculated by Debye-Scherrer formula for (100), (002) and (101) peaks with PANalytical HighScore Plus program. The specific surface area has been determined by the Brunauer-Emmett-Teller (BET) method at 77 K using an ASAP2020 Physisorption Analyzer. Thermogravimetric (TGA) measurements have been performed in order to evaluate the efficiency of the washing steps of the as-prepared ZnO colloidal solutions (Setaram 92-16.18 Thermobalance). The measure of weight loss upon heating of previously

washed samples is attributed to the residual ligands elimination (ramp 10°C/min, temperature step between 25 and 550°C, air).

ZnO sensing films deposition and conductivity measurements

The as-prepared and washed ZnO nanoparticles have been dispersed in ethanol (Sigma Aldrich) with a concentration of 0.5 % wt. of ZnO. ZnO sensing layers have been drop deposited on a miniaturized micromachined silicon substrate by a generic ink-jet method (Autodrop AD system, Microdrop AG). The silicon platform (Fig. 1) has been developed by the Laboratoire d'Analyse et d'Architecture des Systèmes, LAAS-CNRS, MICA team. The die size is 2×2 mm, and presents a 1.4 µm thick dielectric membrane (SiN_x/SiO_2) designed for the thermal insulation of the heated zone. The platinum heater with a spiral shape, is buried between the bottom dielectric membrane and a top layer of silicon dioxide. This heater structure stands a temperature up to 700°C, and the power consumption is as low as of 55 mW at an operating temperature of 500°C. The platinum interdigitated electrodes for the resistance measure of the sensitive layer are deposited in a final step on top of the SiO_2 insulating layer. A distance of 10 µm between each electrode pole provides a reliable contact with sensing layers and offers the access to highly resistive materials measurements (Menini et al., 2008).
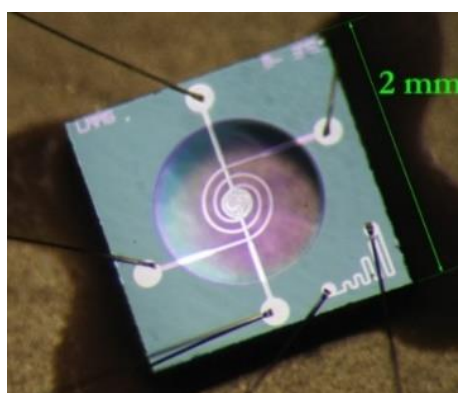

Fig. 1 Image of the gas sensor silicon platform (LAAS).

Gas tests have been performed using a PC controlled setup composed of different gas bottles connected to mass flow controllers (QualiFlow) driven by an Agilent Data Acquisition/Switch Unit 34970A. Sensors are placed in a measurement cell equipped with humidity and temperature sensors. The integrated heaters are controlled by a HP6642A system. A National Instruments 6035E electronic card establishes the connection between the computing unit and the measurement cell. Freshly prepared sensors are initially prepared in ambient air by *in situ* annealing of the sensitive layer up to 550°C. The sensors resistance is then stabilized by an operation at 500°C under a continuous flow (1L.min^{-1}) of synthetic air during several hours. Finally, the sensors are exposed to 100 ppm and 490 ppm CO, 100 and 400 ppm C_3H_8, and 19 ppm NH_3 at operating temperatures of 500°C, 400°C, and 340°C. The relative humidity (RH) is kept constant at 50%, and the total gas flow rate is 1 L.min^{-1}. Results reported here have been performed by using at least 3 sensors of each category, *i.e.* ZnO NP, CL and NR.

Results and Discussion

Characterization of ZnO nanoparticles

The TEM images of the ZnO nanoparticles with different morphology are presented on Fig. 2. The controlled hydrolysis of the dicyclohexylzinc (II) precursor in THF solution without any ligands leads to the formation of cloud-like (ZnO CL) structures (30-100 nm) assembled from agglomerated ZnO nanoparticles (2-3 nm) (Fig. 2a). Isotropic nanoparticles (ZnO NP) with an average diameter of 5.1±1.1 nm (Fig. 2b) have been obtained by the controlled hydrolysis of [ZnCy2] in THF solution and in the presence of octylamine. Well-defined nanorods (ZnO NR) with an average diameter of 5.3±1.0 nm and a length of 21±6 nm (Fig. 2c) are formed in the case of a [ZnCy2] hydrolysis in pure octylamine medium. The mean diameter of the particles is evaluated by fitting of the histogram with a Gaussian curve. The first value corresponds to the center of the peak whereas the second one corresponds to twice the standard deviation of the Gaussian distribution or approximately 0.849 the width of the peak at half-height.

HRTEM images of NR and NP structures are presented on Fig. S1a and 1b. On S1a picture, two NP particles are laying on their basal (0001) face, whereas the third one is placed laterally. Figure S1b shows several ZnO NB laying along their lateral faces. All particles are monocrystalline.
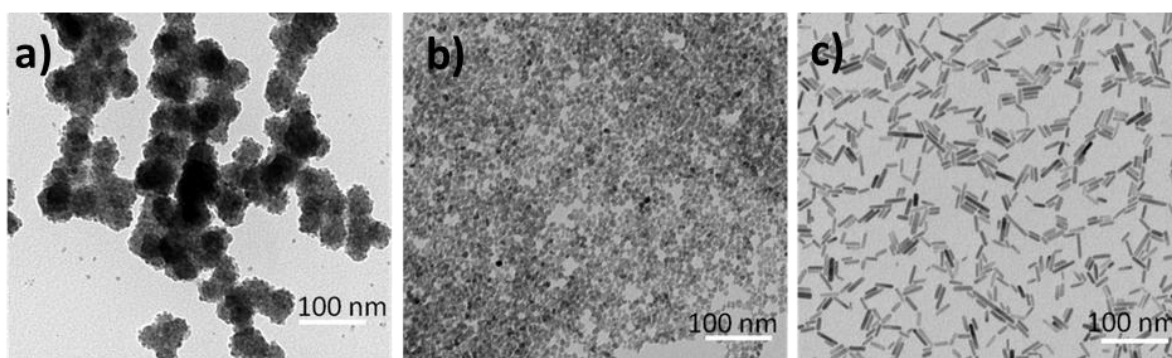

Fig. 2 TEM images of ZnO nanoparticles with different morphology:
(**a**) ZnO CL, (**b**) ZnO NP, (**c**) ZnO NR.

The X-rays diffractograms of as-prepared and washed with acetone ZnO nanostructures are presented on Fig. 3. All the samples contain only hexagonal zincite phase (JCPDS 26-1451). A sharp and high intensity diffraction peak corresponding to (002) plane (2θ = 34.6°) is observed on the XRD spectrum of ZnO NR. These results are characteristic of the growth of the crystal along the *c* crystallographic axe of the Wurzite structure. In contrast and as expected, this is not observed for ZnO NP or ZnO CL. The average crystallite size values calculated by the Debye-Sherrer formula are respectively 3 nm and 7 nm for ZnO CL and ZnO NP. In the case of ZnO NR the crystallite size is around 5 nm for the transversal axis and 26 nm for the longitudinal one. These results confirm the growth of ZnO nanorods along of preferential c-axis of the zincite phase and are in accordance with previous data (Chaudret et al., 2005).

According to the thermogravimetric (TGA) analysis, the washed sample of ZnO NP contains a residual level of *c.a.* 0.1 eq. octylamine, *i.e.* 10 % molar (Fig. S2a). Surprisingly, in the case of ZnO NR the washing with acetone is less effective, since the sample still contains 0.2 eq. of octylamine after the same washing procedure (Fig. S2b). These results can be explained by stronger Van-der-Waals (hydrophobic) interactions between alkyl chains of amines and ZnO nanorods as compared to the isotropic nanoparticles. To support this hypothesis, we have previously demonstrated that the amine ligands are preferentially coordinated on the lateral faces of ZnO nanocrystals (Coppel et al., 2012). Anyway, this slightly higher level of residual amine coordinated to ZnO NR does not impact the sensor performance since the *in-situ* heating up to 550°C is efficient enough to fully remove all organic residues from the sensitive layer.
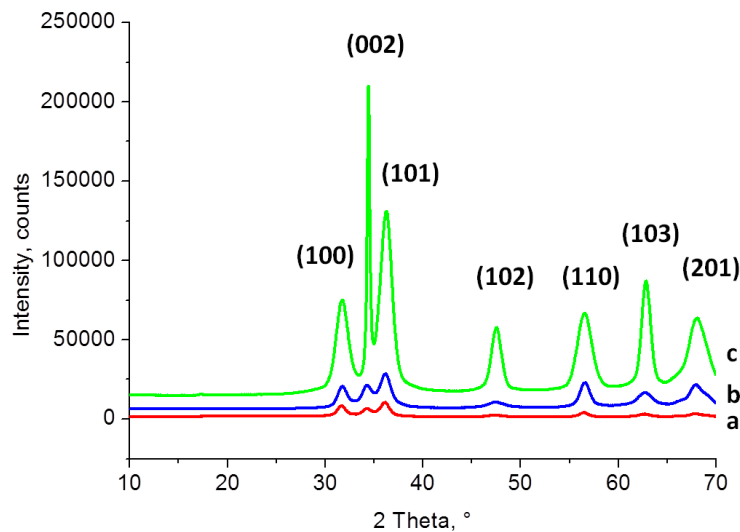
Fig. 3 X-rays diffractograms of ZnO nanoparticles with different morphology:
(**a**) ZnO CL, (**b**) ZnO NP, (**c**) ZnO NR.

Properties of ZnO layers

The ZnO nanoparticles have been deposited as gas sensitive layers on silicon chips by an inkjet method. After deposition, the layers have been *in situ* annealed by operating the integrated Pt heater up to 550°C. The annealing and stabilization temperature profile is presented in Fig. 4. The long intermediate steps performed at low temperature (150°-350°C) allow the slow removal of solvent and ligand traces from the sensitive layers. High quality layers with ZnO thickness of 5-10 µm without large cracks or delamination are obtained (Fig. 5a). The microstructure of the layers was investigated by SEM-FEG observations. It is noteworthy that, the morphology of ZnO nanoparticles is retained on the silicon platform even after *in-situ* thermal treatment up to 550°C (Fig. 5b, c, d).

Gas sensing properties towards various reducing gases, namely 100 ppm and 490 ppm CO, 100 and 400 ppm C_3H_8, and 19 ppm NH_3 have been studied in the temperature range of 340°- 500°C and relative humidity (RH) of 50%. These concentrations have been chosen in a range which is of interest for usual air quality standards (OSHA Permissible Exposure Limits). The representative results of the temperature effect on the sensors response are shown on Fig. 6. The electrical resistance of the different ZnO sensitive layers decreases with the operating temperature and reaches its minimum value of few MOhms at 500°C. Moreover, at this temperature, the resistance of the different sensors decreases in the following order: ZnO NR > ZnO NP > ZnO CL. The resistance decreases also in the presence of reducing gases. This is a characteristic behavior of the n-type semiconductor sensors. It is noteworthy that, the sensors have shown fast and reversible responses to tested gases. However, no performance tests have been carried out below 340°C because of the too slow reaction times as well as too high sensors resistance at low temperature. Resistance is measured before and after sensors exposure to reducing gas mixture and the normalized response (%) to each gas is calculated as $Rn (\%) = (R_{air} - R_{gas})/R_{air}*100$. Typical values of the normalized sensors response to reducing gases at different temperature are displayed on Fig. 7. In order to quantitatively estimate the selectivity of gas detection, the selectivity coefficient (K_{sel}), which

corresponds to the ratio of the sensors normalized response to different gases ($K_{sel} = R_{gas1}/R_{gas2}$), has been also calculated. We assume that a K_{sel} coefficient with a value higher than 2 corresponds to a selective response to a given gas.
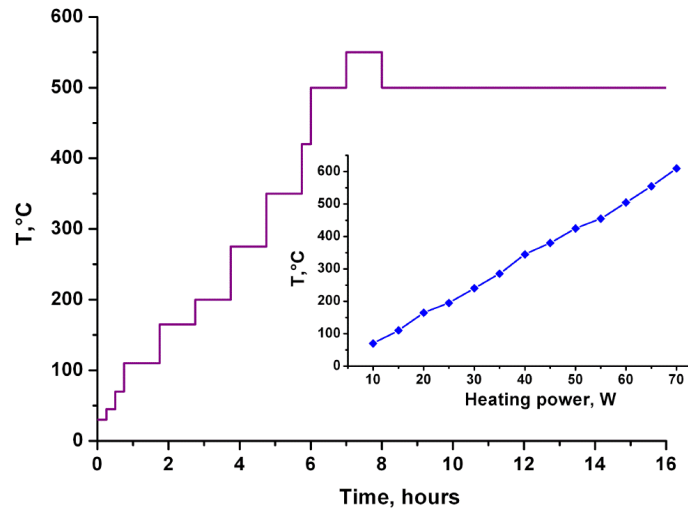

Fig. 4 Temperature profile of the annealing protocol of ZnO sensing layers (insert: relation between heating power and sensor temperature).
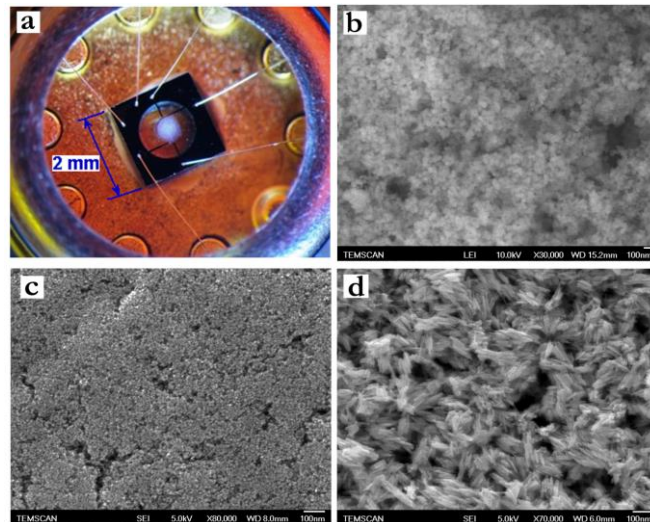

Fig. 5 (**a**) Picture of a sensor covered with ZnO sensitive layer and SEM-FEG images of (**b**) ZnO CL, (**c**) ZnO NP, and (**d**) ZnO NR sensitive layers after *in-situ* thermal treatment up to 550°C.
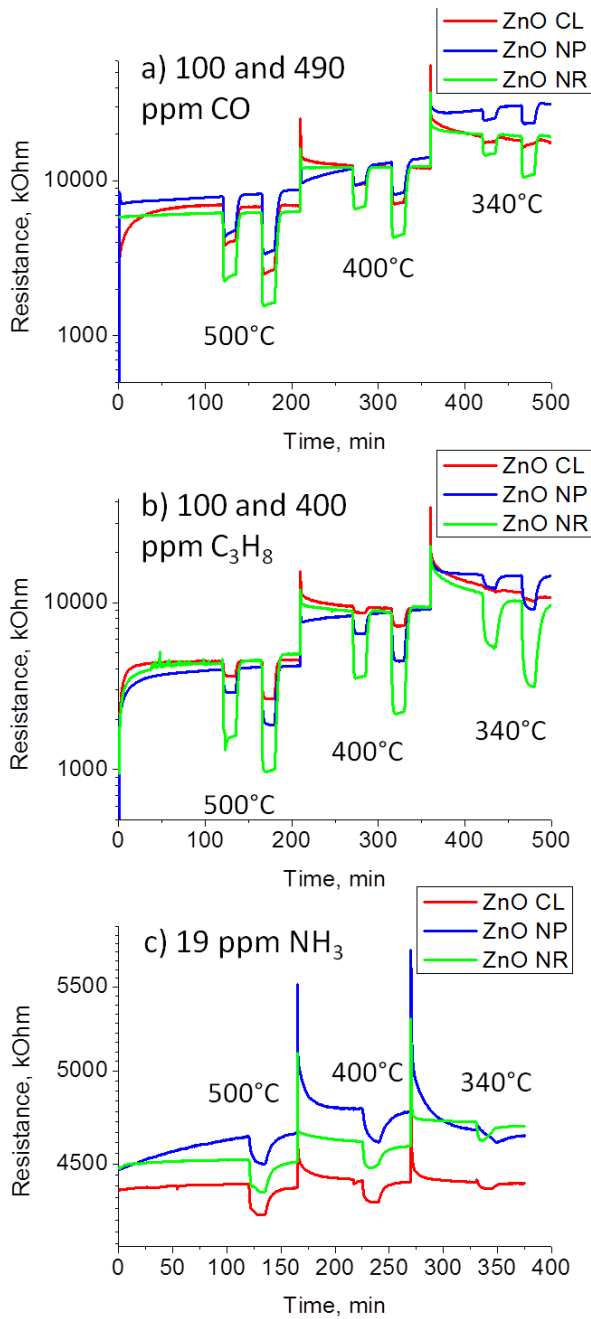
Fig. 6 Typical sensors response obtained for ZnO CL, NP, and NR at different operating temperatures (500, 400 and 340°C) and at relative humidity of 50% (Y scale in log plot). (**a**) 100 and 490 ppm CO, (**b**) 100 and 400 ppm C_3H_8, (**c**) 19 ppm NH_3.

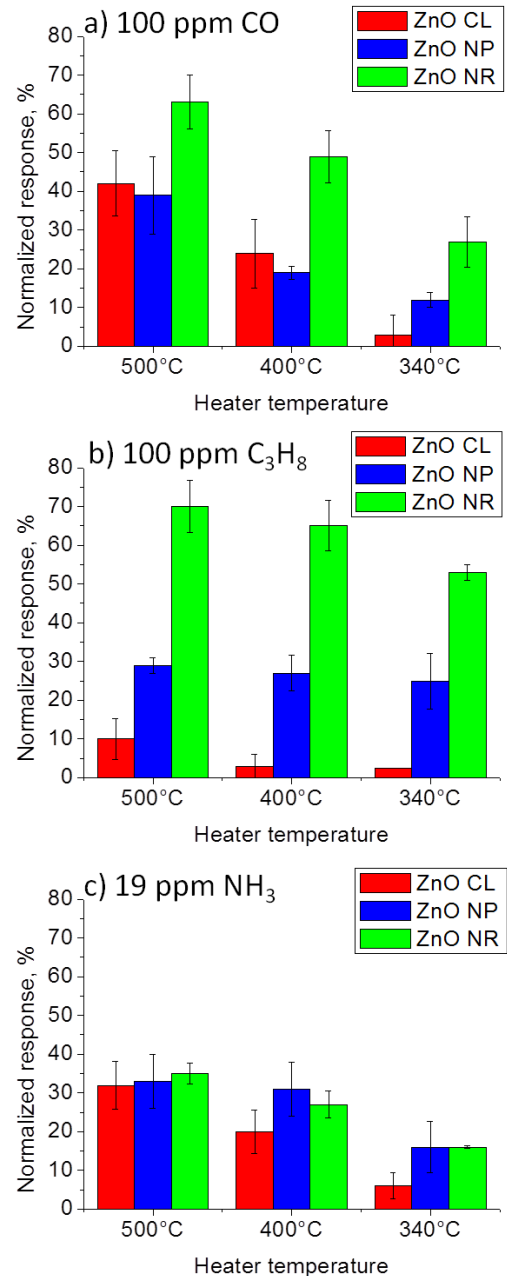**Fig. 7** Normalized responses obtained for ZnO CL, NP and NR at different operating temperatures (500, 400 and 340°C) and at relative humidity of 50%. (**a**) 100 ppm CO, (**b**) 100 ppm C_3H_8, (**c**) 19 ppm NH_3.

Undeniably, the most important result is that the nanostructure of ZnO layers influences the sensors response (Fig. 6 and Fig. 7). The **ZnO NR** sensors show the highest sensitivity to all tested gases. The

optimum responses to 100 ppm C_3H_8 are obtained at 500°C and 400°C (Rn=70 and Rn=65%, respectively). However, the response towards this gas remains high even at lower operating temperature (Rn=53% at 340°C). The highest response to 100 ppm CO has also been achieved with ZnO NR operated at 500°C (R_n=63%). The response towards this gas decreases slightly with temperature diminution (R_n=49% at 400°C and Rn=27% at 340°C). The best response to 19 ppm NH_3 has also been obtained with ZnO NR (R_n=35% at 500°C), but the other sensors categories are very close to this level (R_n=33% and 32% for ZnO NP and ZnO CL, respectively). The response towards NH_3 also decreases with temperature lowering (R_n=27% at 400°C and Rn=16% at 340°C). These results suggest that the ZnO NR sensors show good selectivity for C_3H_8 relatively to NH_3 at all tested temperatures. Indeed, $K_{sel\ C3H8/NH3}$ at 500, 400 and 340°C is equal to 2.0, 2.4 and 3.3, respectively. Additionally, at the lowest temperature of 340°C the sensors exhibit a rather satisfying selectivity for C_3H_8 versus CO ($K_{sel\ C3H8/CO}$=2.0). Consequently, the ZnO NR sensors can be used for sensitive and selective C_3H_8 detection in the presence CO and NH_3 if they are operated at 340°C.

The **ZnO NP** sensors show the same response to 100 ppm C_3H_8 whatever the operating temperature, *i.e.* the response of the sensors only slightly varies from R_n=29% to Rn=25 % when decreasing the temperature from 500 to 340°C. The response to 100 ppm CO is much more affected by the operating temperature since the response drops from R_n=39% at 500°C to only R_n=12% at 340°C. Therefore, the ZnO NP sensors show slight improvement of selectivity between C_3H_8 and CO by simply varying the operating temperature ($K_{sel\ C3H8/CO}$=0.7 at 500°C and 2.1 at 340°C). The response to 19 ppm NH_3 is at a similar level as compared to the ZnO NR sensors. Consequently, the selectivity for C_3H_8 or CO gases relatively to NH_3 is always poor with the ZnO NP sensors. No significant response variations are obtained between NH_3 and the other investigated gases within the range of operating temperature.

From all tested morphologies, **ZnO CL** category shows very low response to 100 ppm C_3H_8, which varies from Rn=10% at 500°C to Rn=2.5% at 340°C. The response to 100 ppm CO is comparable to ZnO NP category and varies from R_n =42% at 500°C to R_n=3% at 340°C. The response to 19 ppm NH_3 is at a similar level as compared to ZnO NP and NR sensors. Thus, the ZnO CL sensors have high selectivity for NH_3 or CO relatively to C_3H_8. Indeed, $K_{sel\ NH3/C3H8}$ at 500, 400 and 340°C is equal to 3.2, 6.7, and 2.4, respectively. In addition, $K_{sel\ CO/C3H8}$ is equal to 4.2, 7.0, and 1.2, respectively. Therefore, the ZnO CL sensors can be used for selective detection of NH_3 or CO in the presence of C_3H_8, especially if the sensors are operated at the mean temperature of 400°C.

In summary, the ZnO NR sensors present the best sensitivity to 100 ppm CO or C_3H_8. Additionally, these sensors exhibit good selectivity towards C_3H_8 relatively to CO and NH_3 when operated at 340°C. The responses of ZnO NP sensors lay at a mean level. They show a CO sensitivity similar to the level obtained with ZnO CL, but they display a higher response to C_3H_8. From all tested morphologies, ZnO NP exhibit the weakest selectivity between investigated gases. Moreover, the ZnO CL category presents the best selectivity for NH_3 or CO versus C_3H_8 at an operating temperature of 400°C. The specific surface area of these different ZnO nanostructures has been measured by the BET method. ZnO NR presents a lower (31.6 $m^2.g^{-1}$), specific surface than ZnO NP (47.9 $m^2.g^{-1}$) or CL (41.2 $m^2.g^{-1}$). Therefore, high sensitivity of the ZnO NR is not related to this parameter and the differences in sensors performance must be correlated to the exposed crystalline faces and their reactivity to the target molecules.

The prismatic faces (($10\bar{1}0$) and ($11\bar{2}0$)) of ZnO NR crystal, which are terminated by both O and Zn atoms, geometrically represent at least 90% of the total surface of the crystal. In this study, the highest sensor response to CO is obtained with ZnO NR morphology (Fig. 7). This result suggests a higher adsorption affinity of CO molecules to prismatic face of ZnO nanocrystals (Scarano et al. 1992). Since CO reaction on MOS sensors surface always rely on chemisorbed O^- oxygen species (Goepel and

Schierbaum, 1995), this suggests that the lateral faces of ZnO NR present a higher ratio of chemisorbed oxygen than the basal surfaces.

In the case of ZnO NP and CL, where lateral and basal faces are equivalently exposed, the response to CO gas is much lower than for ZnO NR. From this result it can be hypothesized that the higher ratio of basal faces are less favorable to CO adsorption compared to lateral faces. An experimental answer to this question could be resolved by the preparation of new ZnO nanostructures displaying extended areas of basal planes and a minimum c- axis length.

As shown on Fig. 7, sensors based on ZnO NP and especially on ZnO NR are more sensitive to 100 ppm C_3H_8 (respectively $R_n = 39\%$ and 70% at $500°C$) than ZnO CL ($R_n = 10\%$ at $500°C$). Therefore, we conclude that both basal and especially lateral faces are involved in the reactivity of ZnO to C_3H_8. It can be supposed that the poor cristallinity of CL sensors type (Fig. 3) conducts to very unfavorable adsorption conditions for propane (Katoch et al., 2013).

The sensors responses to 19 ppm NH_3 at $500°C$ are rather similar for all ZnO categories. However the temperature influence is more pronounced for the ZnO CL sensors than for the others morphologies. At $340°C$ the ZnO CL sensors have lost almost all their reactivity to all gases, whereas the more crystalline samples (NR and NP) still retain significant levels of responses ($R_n > 10\%$). Contrarily to C_3H_8, NH_3 is a polar molecule and a strong Lewis base which preferentially adsorbs at metal-ionic sites (Lewis acid sites) on metal-oxide surfaces (Ozawa et al., 2009). A higher ratio of Lewis acid sites (Zn atoms) should be assumed in the case of ZnO CL at high temperature ($500°C$). Finally, the sensitivity of the ZnO sensors to reducing gases can be tuned by the use of nanoparticles with very distinct morphology. Taking advantage of the temperature-dependent selectivity of each sensor, and with the help of a mathematical treatment of their signals (such as Principal Component Analysis), a sensors system dedicated to the recognition of gaseous components in a complex mixture could be built with a set of different morphology ZnO sensitive layers.

Conclusions

In this paper, the organometallic synthesis route has been employed to yield ZnO nanoparticles with very distinct morphologies. Their response to three different reducing gases, namely, CO, C_3H_8 and NH_3 has been measured and compared. It has clearly been established that the morphology of ZnO nanostructures significantly influences the sensors gases responses and therefore offers a possible selectivity improvement way for gas sensing device. The sensors based on ZnO CL structures present the highest selectivity for CO or NH_3 relatively to C_3H_8 when operating at $400°C$. ZnO NR sensors display a high response to all tested gases with an optimum selectivity for C_3H_8 comparably to CO and NH_3 when operating at $340°C$. ZnO NP layers present a mean response level to all tested gases. However, this category presents the best stability of the response for C_3H_8 between 340 to $500°C$. The influence of ZnO morphology on sensing behavior is explained by the variation of the nature of the crystalline faces of the ZnO structure exposed to the gas phase. In conclusion, this study is the first step dedicated to the preparation of a multisensor system based on chemoresistive layers with a single chemical composition, but with specific morphologies and different operating temperatures. New experiments are underway in order to evaluate the response and selectivity of the various ZnO sensing layers with mixtures of reducing gases.

Acknowledgments

Author Contributions

All authors contributed equally to the reported research and writing of the paper.

Conflicts of Interest

The authors declare no conflict of interest.

References

Bai, S.; Liu, X.; Li, D.; Chen, S.; Luo, R.; Chen, A. Synthesis of ZnO nanorods and its application in NO_2 sensors. *Sens. Actuat. B* 2011, 153(1), 110-116.

Benkstein, K. D.; Raman, B.; Lahr, D. L.; Bonevich, J. E.; Semancik, S. Inducing analytical orthogonality in tungsten oxide-based microsensors using materials structure and dynamic temperature control. *Sens. Actuat. B* 2009, B137 (1), 48-55.

Chand Singh, R., Singh, O., Pal Singh, M., Singh Chandi, P. Synthesis of zinc oxide nanorods and nanoparticles by chemical route and their comparative study as ethanol sensors. *Sens. Actuat*. B 2008, (135), 352-357.

Chaudret, B. Organometallic approach to nanoparticles synthesis and self-organization. *C. R. Physique* 2005, 6(1), 117-131.

Chen, D.; Hou, X.; Li, T.; Fan, D.; Wang, H.; Li, X.; Xu, H.; Lu, H.; Zhang, R.; Sun, J. Effects of morphologies on acetone-sensing properties of tungsten trioxide nanocrystals. *Sens. Actuat. B* 2011, 153(2), 373-381.

Cobden, P. D., Nieuwenhuys, B. E., Gorodetskii, V.V. Adsorption of some small molecules on a Pd field emitter. *Appl. Catal. A* 1999, 188(1-2), 69-77.

Coppel, Y.; Spataro, G.; Pagès, C., Chaudret, B., Maisonnat, A.; Kahn, M. L. Full characterization of colloidal solutions of long-alkyl-chain-amine-stabilized ZnO nanoparticles by NMR spectroscopy: Surface state, equilibria, and affinity. *Chem. Eur. J.* 2012, 18(17), 5384-5393.

Geng, B.; Fang, C.; Zhan, F.; Yu, N. Synthesis of polyhedral $ZnSnO_3$ microcrystals with controlled exposed facets and their selective gas-sensing properties. *Small* 2008, 4(9), 1337-1343.

Goepel, W.; Schierbaum, K. D. SnO_2 sensors: current status and future prospects. *Sens. Actuat. B* 1995, 26(1-3), 1-12.

Gupta, S.K.; Joshi, A.; Kaur, M. Development of gas sensors using ZnO nanostructures. *J. Chem. Soc.* 2010, 122(1), 57-62.

Heilig, A.; Weimar, U.; Schweizer-Berberich, M.; Gardner, J. W.; Gopel, W. Gas identification by modulating temperatures of SnO_2-based thick film sensors. *Sensors and Actuators B* 1997, 43(1-3), 45-51. Kahn, M.L.; Collière V., Senocq, F.; Maisonnat, A.; Chaudret, B. Size- and shape-control of crystalline zinc oxide nanoparticles: a new organometallic synthetic method. *Adv. Funct. Mater.* 2005, 15(3), 458-468.

Katoch, A., Sun, G.-J., Choi, S.-W., Byun, J.-H. Kim, S. S. Competitive influence of grain size and crystallinity on gas sensing performances of ZnO nanofibers, *Sens. Actuat. B* 2013, 185, 411-416.

Kolodziejczak-Radzimska, A.; Jesionowski, T. ZnO Oxide-from synthesis to application: a review. *Materials* 2014, 7, 2833-2881.

Le, V. T.; Le, T. N. L.; Nguyen, V. H. Comparative study of gas sensor performance of SnO_2 nanowires and their hierarchical nanostructures. *Sens. Actuat. B* 2010, 150(1), 112-119.

Liao, F.; Huang, Y.; Ge, J.; Zheng, W.; Tedsree, K.; Collier, P.; Hong, X. Morphology-dependent interactions of ZnO with Cu nanoparticles at the materials' interface in selective hydrogenation of CO_2 to CH_3OH. *Angew. Chem., Int. Ed.* 2011, 50 (9), 2162-2165.

Liu, X.; Liu, J.; Chang, Z.; Sun, X.; Li, Y. Crystal plane effect of Fe_2O_3 with various morphologies on CO catalytic oxidation. *Catal. Commun.* 2011, 12(6), 530-534.

Menini, Ph.; Chalabi, H.; Yaboue, N. P.; Scheid, E.; Conedera, V.; Salvagnac, L.; Aguir, K. High performances of new microhotplate for gas sensors. *Eurosensors XXII*, Dresde (Allemagne), Septembre 2008.

OSHA Permissible Exposure Limits (PELs), https://www.osha.gov/dsg/topics/pel/

Ozawa, K.; Hasagawa, T.; Edamoto, K.; Takahashi, K.; Kamada, M. Adsorption state and molecular orientation of ammonia on ZnO ($10\overline{1}0$) studied by photoelectron spectroscopy and near-Edge X-ray Absorption Fine Structure Spectroscopy. *J. Phys. Chem. B* 2002, 106(36), 9380-9386.

Rai, P., Kwak, W.-K., Yu, Y.-T. Solvothermal synthesis of ZnO nanostructures and their morphology-dependent gas-sensing properties. *Appl. Mater. Interfaces* 2013, (5), 3026−3032.

Rout, C.S.; Hegde, M.; Govindaraj, A.; Rao, C. N. R. Ammonia sensors based on metal oxide nanostructures. *Nanotechnology* 2007, 18(20), 205504/1-205504/9.

Ryzhikov, A., Labeau, M.; Gaskov, A. Al_2O_3 (M=Pt, Ru) catalytic membranes for selective semiconductor gas sensors. *Sens. Actuat. B* 2005, 109(1), 91-96.

Scarano, D., Spoto, G., Bordiga, S., Zecchina, A. Lateral interactions in CO adlayers on prismatic ZnO faces: a FTIR and HRTEM study. *Surf. Sci.* 1992, 276, 281-298

Shaalan, N.M.; Yamazaki, T.; Kikuta, T. Influence of morphology and structure geometry on NO2 gas-sensing characteristics of SnO_2 nanostructures synthesized via a thermal evaporation method. *Sens. Actuat. B* 2011, 153(1), 11-16.

Simon, I.; Barsan, N.; Bauer, M.; Weimar, U. Micromachined metal oxide gas sensors: opportunities to improve sensor performance. *Sens. Actuat. B* 2001, 73(1), 1-26.

Wang, D.; Kang, Y.; Doan-Nguyen, V.; Chen, J.; Kungas, R.; Wieder, N. L.; Bakhmutsky, K.; Gorte, R. J.; Murray, C. B. Synthesis and oxygen storage capacity of two-dimensional ceria nanocrystals. *Angew. Chem., Int. Ed.* 2011, 50(19), p. 4378-4381.

Weimar, U.; Goepel, W. Chemical imaging: II. Trends in practical multiparameter sensor systems. *Sens. Actuat. B* 1998, 52(1-2), 143-161.

Wu, C.; Zhu, X.; OuYang, C.; Xie, Y. Synthesis of Hematite (α-Fe_2O_3) Nanorods: diameter-size and shape tffects on their applications in magnetism, lithium ion battery, and gas sensors. *J. Phys. Chem. B* 2006, 110(36), 17806-17812.

Xu, J., Zhang, Y.; Chen, Y.; Xiang, Q.; Pan, Q.; Shi, L. Uniform ZnO nanorods can be used to improve the response of ZnO gas sensor. *Mater. Sci. Eng. B* 2008, 150(1), 55-60.

Yamazoe, N.; Kurokawa, Y.; Seiyama, T. Effects of additives on semiconductor gas sensors. *Sens. Actuat.* 1983, 4(2), 283-289.

Yu, L.; Fan, X.; Qi, L.; Ma, L.; Yan, W. Dependence of morphologies for SnO_2 nanostructures on their sensing property. *Appl. Surf. Sci.* 2011, 257(7), 3140-3144.

Zhang, W.-D.; Zhang, W.-H.; Ma, X.-Y. Tunable ZnO nanostructures for ethanol sensing. *J. Mater. Sci.* 2009, 44(17), 4677-4682.

Zhao, Q., Shen, Q., Yang, F., Zhao, H., Liu, B., Liang, Q., Wei, A., Yang, H., Liu, S. Direct growth of ZnO nanodisk networks with an exposed (0001) facet on Au comb-shaped interdigitating electrodes and the enhanced gas-sensing property of polar (0001) surfaces. *Sens. Actuat*. B 2014, 195, 71-79.